Applied Catalysis B: Environmental 185 (2016) 150–162

Contents lists available at ScienceDirect

Applied Catalysis B: Environmental

journal homepage: www.elsevier.com/locate/apcatb

# Castles fall from inside: Evidence for dominant internal photo-catalytic mechanisms during treatment of *Saccharomyces cerevisiae* by photo-Fenton at near-neutral pH

Stefanos Giannakis[a], Cristina Ruales-Lonfat[a], Sami Rtimi[a], Sana Thabet[b], Pascale Cotton[b], César Pulgarin[a,*]

[a] SB, ISIC, Group of Advanced Oxidation Processes, Ecole Polytechnique Fédérale de Lausanne (EPFL), Station 6, 1015 Lausanne, Switzerland
[b] Université de Lyon, Université Lyon1, CNRS-UCB-INSA-BCS, UMR 5240, Génétique Moléculaire des Levures, Microbiologie, Adaptation et Pathogénie, Domaine scientifique de la Doua, 10 rue Raphaël Dubois, bâtiment Lwoff, F-69626 Villeurbanne, France

ARTICLE INFO

*Article history:*
Received 2 November 2015
Received in revised form 4 December 2015
Accepted 10 December 2015
Available online 14 December 2015

*Keywords:*
Near-neutral photo-Fenton
*Saccharomyces cerevisiae*
Inactivation mechanism
DNA damage
Cytoplasmic and cell wall proteins

ABSTRACT

In this work, the antimicrobial effects of the photo-Fenton process on yeast cells were tested (*Saccharomyces cerevisiae*), an essential eukaryotic unicellular model of living cells. Near-neutral pH was used in all studies, while iron sulfate and iron citrate were evaluated as iron sources during *S. cerevisiae* photo-Fenton inactivation under simulated solar light ($h\nu/H_2O_2/Fe$). The following indicators were monitored to decrypt the mechanism of yeast inactivation by neutral photo-Fenton process: cell viability by flow cytometry, damage at DNA level, as well as intracellular and extracellular proteins, assessed by gel electrophoresis. A significant loss of cultivability was monitored through the application of all the different photo-Fenton systems, attributed to the oxidative stresses applied. The mechanisms involved were the homogeneous action of dissolved iron and the heterogeneous action mode of iron oxides. The DNA and protein analyses indicated drastic intracellular damages, while external macromolecules (cell wall and membrane proteins) showed limited degradation. This marked internal photocatalytic processes as the main inactivation mechanism in *S. cerevisiae*. Different pathways are proposed, forming a general process of inactivation by the near-neutral photo-Fenton systems.



## 1. Introduction

Historically, one of the biggest side-effects of urbanization, was the high concentration of inhabitants in relatively small areas, which in turn created massive flows of wastewater. It was not until after the Industrial Revolution that the these wastes started to become a threat against the environment, since up to that point, the self-cleaning capacity of natural water bodies was able to regulate the incoming nutrient, organic and inorganic pollution. The last decades, apart from the chemical constituents, a systematic effort to upgrade the wastewater treatment plants has been undertaken, in order to eliminate microbiological contaminants contained in wastewater. As first approaches, chlorination, peracetic acid and other chemical methods were employed [1], gradually replaced by more eco-friendly methods (such as UV or ozonation) due to the lower harmful by-products connected with their application.

Moreover, hospital wastewater has been categorized as a main contributor of chemical substances (drugs, wastes) [2] and microbiological agents normally not encountered in municipal wastewater, such as high concentration of antibiotic resistant bacteria, viruses, yeasts or fungi [3–5]. The similar origin of wastewater in health facilities led the practitioners to apply one sterilization step before leading the treated wastewater in the municipal wastewater treatment plants [6]. During the last years in Europe, there is an increasing demand of treatment plants specifically designed for hospitals, taking into account the special form of pollution contained [7]. Nevertheless, in less favorable regions of the world, these wastewater treatment plant facilities are either a luxury, non-existing or have never operated properly. As a result, the wastewater is directly discharged into nature and the natural water bodies are transformed into disease carriers. Bacterial induced illnesses, such as diarrhea, viral or fungal-related infections have been

*Abbreviations:* AOPs, advanced oxidation processes; CAT, catalase; CFDA5, carboxyfluorescein diacetate; CPDs, cyclobutane pyrimidine dimers; DNA, deoxyribonucleic acid; Fe/S, iron–sulfur; hv, light; LMCT, ligand-to-metal charge transfer; PI, propidium iodide; ROS, reactive oxygen species; SDS-PAGE, polyacrylamide gel electrophoresis; SOD, superoxide dismutase; UV, ultraviolet.

* Corresponding author.
*E-mail address:* cesar.pulgarin@epfl.ch (C. Pulgarin).

http://dx.doi.org/10.1016/j.apcatb.2015.12.016
0926-3373/

encountered, problems craving a simple, cheap and sustainable solution [8,9].

The advanced oxidation processes (AOPs) have emerged during the last years as a practical and in some cases, easily applicable solution, as a barrier to stop pollution in contaminated drinking water sources. As a common denominator, the extremely oxidative hydroxyl radical is produced, and secondarily, other reactive oxygen species [10]. Ozonation (at basic pH), heterogeneous photocatalysis by $TiO_2$, UV-induced production of HO by the homolytic disruption of $H_2O_2$ and the iron-catalyzed radical induction are some of the most popular AOPs in decontaminating water or wastewater [11,12]. Especially the Fenton reaction, and its photo-enhanced version, gained much merit during the last decade, after the proof of its considerable effectivity at near-neutral pH [13]; in the past, its acidic pH-bound character acted as a limiting step toward its application against microorganism removal. Its low cost and easy application has proven itself a powerful ally in sunny regions around the globe [14,15].

A significant number of studies discuss the efficiency of the Fenton reaction as an antibacterial agent, using most commonly *Escherichia coli*, but also *Enterococci*, and *Salmonella* [14,16–18]. The efficiency of the Fenton reaction was lately tested for the inactivation of viruses, such as MS2Coliphage and Echovirus [19]. Although prokaryotic unicellular microorganisms have been more studied, due to their omnipresence in the environment and their impact on health, expanding works on other groups of microorganisms is necessary. The impact of eukaryotic microorganisms on environment and human health is not negligible. The effects of photocatalysis on fungal cell survival has been showed for environmental species, like *Penicillium*, *Fusarium*, and *Aspergillus* that are frequently recovered from water and soil [20–22] and for yeast species like *Candida* closely associated to human opportunistic infections [23].

In eukaryotic cells, there are significant structural modifications compared to prokaryotes which may facilitate difference in interesting traits, disinfection-wise, such as resistance, higher stress responses and repair mechanisms [24]. A series of photocatalysis studies using $TiO_2$ have focused on *Fusarium solani* as a model of multicellular microbial structure [25,26], and at the unicellular level on *Saccharomyces cerevisiae* as a model for oxidative response [23,27]. It was proven that there is limited penetration of $TiO_2$ nanoparticles into the yeast cell, and that photocatalysis induces the establishment of an intracellular oxidative environment [23]. In bacteria, the effect of an internal Fenton mechanism has been brought to surface [10], complementing the external pathways but yet, it is still unclear how it would act, when yeast cells are the target of the Fenton reaction.

In this work, we have used *S. cerevisiae*, as a model of eukaryotic microorganisms, and photo-Fenton as the antimicrobial AOP. The mechanisms of yeast inactivation by photo-Fenton process at near-neutral pH were investigated. The reactions were fueled by different iron sources, namely iron sulfate and iron citrate, in presence of $H_2O_2$, under simulated solar light. The different inactivation pathways were interpreted by using flow cytometry, and assessment of the damage at both DNA and protein level was also performed. DNA and cell wall protein damages were depicted by electrophoresis, to elucidating the photo-Fenton mode of action.

## 2. Materials and methods

### 2.1. Chemicals

Ferrous sulfate heptahydrate ($FeSO_4{\cdot}7H_2O$) (Riedel-de Haën 99–103.4%); Ferric chloride ($FeCl_3$) (98% carlo erba), Trisodium citrate dihydrate ($Na_3C_6H_5O_7{\cdot}2H_2O$) (99% Merck); Sodium hydrogen carbonate ($NaHCO_3$) (analytical grade, Merck); Hydrogen peroxide ($H_2O_2$) 30% w/v (Riedel de Haën); Titanium (IV) oxysulfate ($TiOSO_4$) (Fluka); Sodium hydroxide (NaOH, 98%) and hydrochloric acid (HCl, 36.5%), were purchased from Sigma–Aldrich, Switzerland. The spin-trap, 5,5-dimethyl-1-pyrroline-*N*-oxide (DMPO), was purchased from Enzo Life Sciences (ELS) AG (Switzerland). All solutions were prepared immediately prior to irradiation with the use of Milli-Q water (18.2 MΩ-cm).

### 2.2. Fe-citrate complex and goethite preparation

Fe-citrate complex was prepared according at modified patent European from Bayer [28]. Ferric chloride (4.1 g) and sodium hydrogen carbonate (3.0 g) were dispersed in 50 mL of distilled water and dissolved therein by stirring. This solution was degassed under vacuum for 2 h followed by constant stirring and Trisodium citrate dihydrate (4.0 g) was added. The color of the solution turned to a pale brown. The solution was stored in the dark for 24 h. Then, 40 mL of methanol was added to the brown solution under constant stirring at 25 °C and a brown precipitate was formed. The resulting solution was centrifuged (5 min at 5000 rpm) to remove the precipitate, and the clear supernatant suspension was separated by filtration. The precipitate was washed with methanol at least three times and dried under vacuum at room temperature. Goethite preparation and characterization was analytically presented in previous works of our group [18].

### 2.3. Yeast strains and growth media

The laboratory strain *S. cerevisiae* (BY4742) was used for all yeast inactivation experiments. The strain was maintained on YPD medium (1% yeast extract, 1% peptone, 2% glucose, 2% agar for plates). Yeast cells were grown in liquid YPD overnight under aerobic conditions with constant shaking at 28 °C. The yeast culture growth was checked by measuring optical density at 600 nm using a spectrophotometer. For all experiments, cell samples were collected at the beginning of the exponential growth phase ($OD_{600}$ = 1,) washed twice and suspended in the photoreactor in 20 mL of sterile ultra-pure (UP) water (Simplicity$^{TM}$, Millipore), resulting into a concentration of $10^7$ cells/mL.

### 2.4. Photo-inactivation experiments

All yeast inactivation experiments were performed in Pyrex reactors (4 cm × 9 cm, 100 mL). The Pyrex reactors containing the yeast suspension in Milli-Q water (approximately $10^7$ CFU/mL) were placed in the dark at 25 °C under magnetic stirring for at least 30 min to let the yeast adapt to the new matrix and to allow the die-off and equilibration of the most stress-sensitive species.

The following systems were analyzed for the inactivation effect on yeast. (i) photo-Fenton process mediated by Fe-citrate (0.6 mg Fe/L) at pH: 6.0 or 7.5; (ii) photo-Fenton process mediated by $FeSO_4$ (0.6 mg Fe/L) at pH: 5.5 and 7.5; and (iii) control experiments: $H_2O_2$/dark; light alone and $H_2O_2$/light. Goethite addition (0.6 mg Fe/L) was assessed complementarily, to assess the function of the iron after its precipitation in the near-neutral environments. In the experiments iron was added to a yeast suspension. Then, the pH was adjusted depending on the experiment. Neighboring near-neutral values were assayed to better investigate the behavior of a system which partially permits soluble Fe and compare with realistic pH. Finally, $H_2O_2$ (10 mg/L) was added to the reactor as the last component.

Experiments were carried out using a solar simulator CPS Suntest System (Heraeus Noblelight, Hanau, Germany). This solar simulator was equipped with a basic uncoated quartz glass light tube, a filter E and an IR screen (neither UVC nor IR is reaching the sample, the intermediate wavelengths are a simulation of the solar

radiation); more information can be found at [37,38]. The irradiance was measured by a spectro-radiometer, Model ILT-900-R (International Light Technologies) and corresponded to 820 W/m$^2$ of light global irradiance (from which ~0.5% UVB, ~5% UVA is emitted). Temperature was monitored and always remained <38 °C.

### 2.5. Cultivability assays

Samples were collected at regular intervals during yeast inactivation reaction. Serial dilutions were immediately made in liquid YPD medium and spread onto YPD agar plates. After 2 days of incubation at 28 °C, the colony forming units (CFU) detected on appropriate dilution plates were counted, in order to determine the concentration of surviving cells. Triplicate plating was performed for each dilution of the samples. All experiments were performed in triplicates and the results presented in the graphs are the average value (<5% statistical error).

### 2.6. Analytical methods

#### 2.6.1. Optical epifluorescence microscopy

Microscopy observations were performed using Axioscop 2 plus Zeiss optical microscope equipped with AxioCam MRm camera. Data were collected using AXioVision software.

Cell viability was investigated using PI (Propidium iodide, Invitrogen, ex/em 490/635 nm) and CFDA-AM dye (Carboxyfluorescein diacetate-acetoxymethyl, ROCH, ex/em 492/517 nm). PI enters only cells with damaged cytoplasmic membranes, whereas CFDA-AM enters all cells and is non-fluorescent until it is cut-off by active cytoplasmic esterases. CFDA-AM reflects cell metabolic activity. Treated cell samples (100 μL) were diluted in PBS to $10^6$ cells/mL. After addition of dyes (1 μg/mL PI and 5 μg/mL CFDA-AM), the mix was incubated for 20 min at 37 °C.

#### 2.6.2. Flow cytometry

Flow cytometry was carried out using FACS CantoII instrument (BD Biosciences) fitted with three lasers: blue (488 nm, aircooled, 20 mW solid state), red (633 nm, 17 mW HeNe) and violet (405 nm, 30 mW solid state). Diffracted light (related to cell surface: Forward scatter FSC) and reflected light (related to granularity: Side scatter SSC) of blue laser, as well as CFDA-AM and PI, were collected. Data from 10,000 cells were collected using FACSDIVA software (6.1.2 version, BD Biosciences).

### 2.7. Biochemical methods

#### 2.7.1. DNA extraction and analysis

Yeast chromosomal DNA was extracted from 2 mL of stationary phase YPG culture at 28 °C and 150 rpm. Cells were collected by centrifugation 30 s at 16000 × *g*, washed in 0.5 mL of sterile water and suspended in 0.2 mL of lysis buffer (2% Triton X-100, 1% SDS, 100 mM NaCl, 10 mM Tris–HCl pH 8,0, 10 mM EDTA pH 8.0). Glass beads (0.5 mm diameter, 0.4 g) and phenol chloroform isoamylalcool (0.2 mL) were then added. Samples were vortexed for 5 min and 0.2 mL TE pH 8.0 (10 mM Tris–HCl pH 8.0, 1 mM EDTA, pH 8.0) was added. After centrifugation (10 min, 16000 × *g*) at room temperature, the supernatant was transferred into a new tube and 0.4 mL chloroform was added. After centrifugation for 2 min at 16000 × *g*, the aqueous phase was transferred and 4 μL of 10 mg/mL RNAse were added. Samples were incubated at 37 °C for 15 min and DNA was precipitated with 1 mL 100% ethanol and incubated for 10 min at −20 °C. After centrifugation (10 min, 16000 g), the pellet was solubilized in 0.4 mL TE pH 8.0. The samples' DNA was quantified using a nanodrop spectrometer at 260 nm. DNA was loaded on a 0.8% agarose gel and separated by electrophoresis according to [29] and visualized under UV irradiation after staining the gels with ethidium bromide (1 μg/mL).

#### 2.7.2. Protein extraction and analysis of protein profiles

To analyze the proteins, the protocol described by Thabet et al. [23] was followed. SDS-PAGE, was performed with 10% (wt/vol) polyacrylamide gels as described by Laemmli [30]. 100 μg of proteins were loaded in each well. LC–MS/MS (HPLC Ultimate 3000; Dionex coupled with LTQ Velos; Thermo Scientific) was used to identify the proteins, followed by discoloration of the bands of interest (by trypsin digestion). A second MS was undertaken for the 10 most significant peaks, and analysis through Proteome Discoverer software (Thermo Electron). The Mascot software (v2.3) was finally used to perform a UniP_Sacchar_cerev search, with the following criteria applied: MS/MS ion search, electrospray ionization (ESI-TRAP), trypsin (digestion enyme), carbamidomethyl and oxidation (modifications), max 2 missed cleavages, peptide and fragment mass tolerance ±1.5 and ±0.6 Da, respectively, ion scores >37, $P < 0.01$ (statistical identification significance).

### 2.8. Experimental planning

The strategy for unveiling the complex inactivation mechanism was as follows. In principal, the photo-Fenton process was stepwise constructed: first light only, then addition of $H_2O_2$ and finally addition of the iron source. This construction was evaluated in three levels: (i) inactivation efficiency measured by cultivability, (ii) localization of the damage (internal, external) and (iii) identification of the targets deriving from the various processes.

## 3. Results and discussion

### 3.1. Cultivability assays—efficiency of treatment

Fig. 1 summarizes the various photocatalytic inactivation tests carried out in the framework of this work. Fig. 1a contains the heterogeneous and homogeneous photocatalytic systems with the respective blank tests, while Fig. 1b and c depict the effect of pH on the efficiency of the (homogeneous) photo-Fenton action.

More specifically, in Fig. 1a the boundary conditions, concerning the oxidative stress applied to *S. cerevisiae* are shown first (✚ trace). Hydrogen peroxide at high concentrations has been reported to have detrimental effect on the survival of *S. cerevisiae* [31]. Normally, $H_2O_2$ acts on its cell wall and plasma membrane, causing carbonylation and thiolation of surface proteins [32–34]. The fungal wall is suggested to protect from diffusion of $H_2O_2$ into the cell of *F. solani* [26], with increasing thickness and efficacy as the cell ages [35]. Here, the control test was performed at 10 mg/L initial $H_2O_2$ concentration. As a result, negligible inactivation was observed during the monitoring period (2 h).

When light was introduced to the system, significant inactivation of yeast cells was initiated (✚ trace). The fungal kingdom is known to be affected by solar [25] or pulsed light [36], which essentially has similar mode of action, but higher intensity. After 30 min of minor inactivation, resembling the shoulder period of inactivation found for *E. coli* [37,38], a linear (at log-scale) pattern was observed, without significant tailing. The necessary dose to initiate the linear inactivation was 72 kJ/m$^2$ and 288 kJ/m$^2$ were required for total inactivation, respectively; compared to other (multicellular) fungi, this is 40% less [39]. The emitted light from the solar simulator includes wavelengths at both UVB and UVA regions. Although UVB is notably less than the UVA (0.5% compared to 5%) its biological effects are significant [40,41]. UV light affects both external sites (cytoplasmic membrane) and internal ones, such as the enzymatic activity and the genomic structure

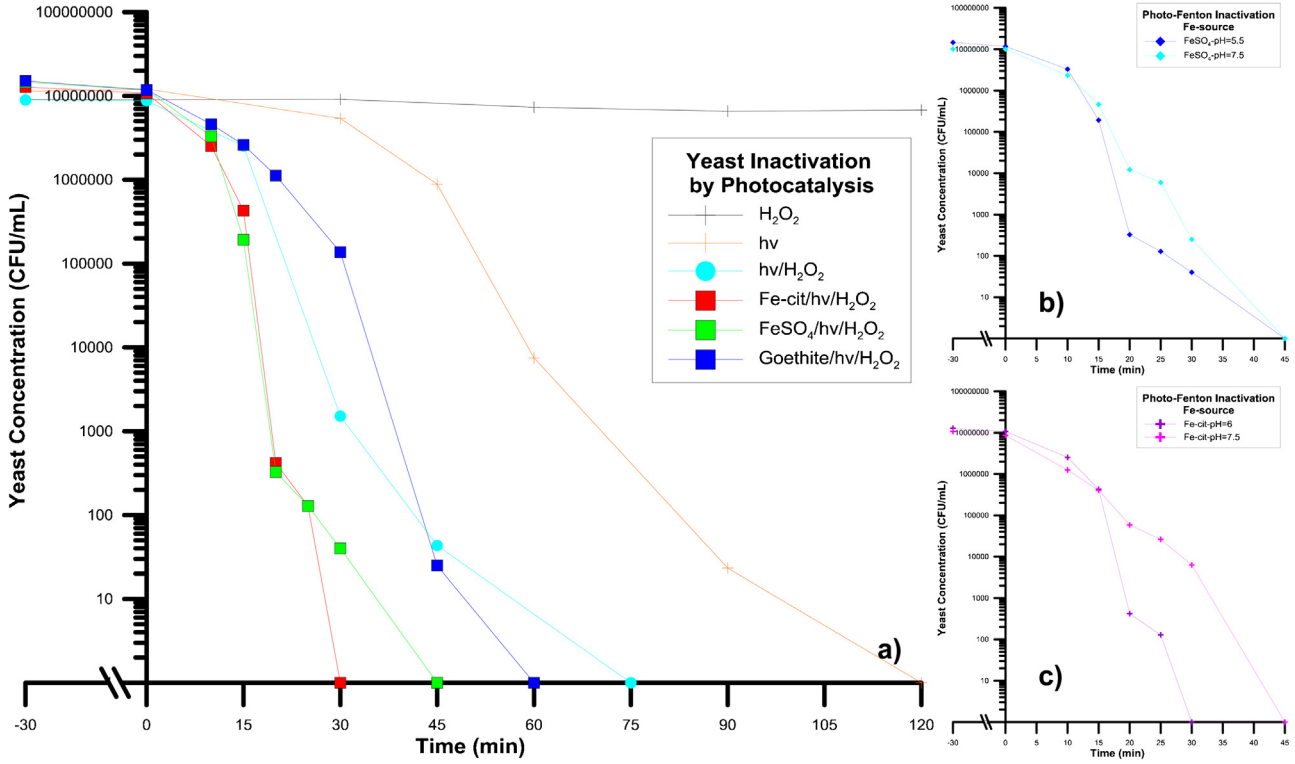


**Fig. 1.** Overview of the photocatalytic inactivation tests and their respective controls. (a) The plots describe the cultivability evolution over time. (b) Comparison between pH 5.5 and 7.5 for the $FeSO_4$-assisted photo-Fenton system. (c) Comparison between pH 6.0 and 7.5 for the iron citrate-assisted photo-Fenton system. Standard deviation: <5%.

[42]. Pfeifer et al. [43] have shown that artificially irradiated cells present a higher percentage of UVB-induced lesions, namely CPDs (cyclobutane pyrimidine dimers), rather than (6–4) photoproducts from type I or II reactions, that UVA is held usually responsible. However, UVA can (i) produce $H_2O_2$ (under certain conditions) by activating oxidases [44] (ii) or, release iron from ferritins [45] and Fe/S clusters [46]; this ends up in initiating an internal (photo) Fenton process. Although DNA has low absorbance in the UVA region (maxima around 260) [47,48]; strand breaks have been reported, supporting this hypothesis, and guanine to cytosine transversions [43]. Finally, apoptotic responses have been reported, and are initiated as a result of disrupted or altered yeast life cycle or UV sensitivity [49,50].

The last control test of the system assessed the combined action of simulated solar light and hydrogen peroxide ( trace). Compared to the simulated solar light test, the required time for 6-log inactivation has decreased almost in half (75 min instead of 120) and the shoulder length has also been decreased to 10 min from 30. In this experiment, notable consumption of $H_2O_2$ was observed compared to the dark test (see Supplementary material Fig. S1). Since it is known that the cleavage of $H_2O_2$ with the subsequent formation of hydroxyl radicals is unlikely to be achieved within the solar spectrum [51], the possible inactivation mechanism is as follows: the action of $H_2O_2$ and UV on the external proteins affects the composition and stability of the membrane, and subsequent regional changes in permeability occur. Since the $H_2O_2$ can now enter the cell, the internal Haber–Weiss reactions are enhanced [16].

The first step of the catalytic cycle involves reduction of ferric ion to ferrous (Eq. (1)):

$$Fe^{3+} + O_2^{\bullet -} \rightarrow Fe^{2+} + O_2 \quad (1)$$

The second step is the Fenton reaction (Eq. (2)):

$$Fe^{2+} + H_2O_2 \rightarrow Fe^{3+} + HO^- + HO^{\bullet} \quad (2)$$

Net reaction (Eq. (3)):

$$O_2^{\bullet -} + H_2O_2 \rightarrow HO^- + HO^{\bullet} + O_2 \quad (3)$$

This hypothesis is reinforced by data acquired by *F. solani*, where notable decrease of $H_2O_2$ occurred, during UVA irradiation [26], and entrance of $H_2O_2$ in the spore was highly probable. The second action mode suggests a damage in the oxidative stress regulation mechanisms in the cell by the action of UV light, such as SOD or CAT, followed by accumulation of ROS into the cell. If the SOD, the responsible for regulation of superoxide radical $O_2^{\bullet -}$ inside the cell is no longer functional, it can lead to the accumulation of$O_2^{\bullet -}$. Superoxide radicals attack the DNA [52], lead to the accumulation of $H_2O_2$ and lately, $O_2^{\bullet -}$has been suggested that in aqueous environments can lead to the formation of hydroxyl radicals ($HO^{\bullet}$) [18,53]. CAT is also strongly affected by light [54] and suspending its functions can cause internal stress by over-accumulation of $H_2O_2$. Once the internal regulation mechanisms have been dropped, the cells cultivability is decreasing dramatically, succumbing to the internal and external stresses initiated by UV and $H_2O_2$.

The remaining inactivation curves describe the photo-assisted Fenton processes undertaken in this study, marked with the square traces. Iron in the form of $FeSO_4$ ( trace), iron citrate ( trace) and iron oxides, as goethite ( trace), were added to the solution 30 min prior to illumination, and $H_2O_2$ addition (and light supply) indicated the initiation of the experimental assay time. According to the different starting forms of iron in the solution, different responses were expected and subsequently monitored in the system. In general, contrary to solar only or solar/$H_2O_2$ systems, an hour or less was required to achieve total inactivation. In addition, apart from the goethite-powered photo-Fenton process, no signif-

icant delay (shoulder) was measured; almost constant inactivation kinetics were observed. An estimated order of efficiency according to the initial iron source was as follows: Goethite < $FeSO_4$ < Citrate.

### 3.1.1. Goethite

Goethite is one of the most abundant forms of iron in nature [18] and can play a significant role in *S. cerevisiae* inactivation as heterogeneous catalyst in presence of $H_2O_2$ [10]. At near-neutral pH, when iron salts (such as the ferrous sulfate used here) are added in presence of $H_2O_2$, zero-charge ferrous complexes [$Fe(OH)_2$] are formed, which are very sensitive to oxidation and rapidly form solid ferric (hydr) oxide compounds, such as goethite and lepidocrocite [10]. Therefore, according to the process described in our previous work, goethite was prepared [18] and used in this study. It is necessary to differentiate the actions attributed to iron oxides, at least for the cultivability assays, as their formation in near-neutral environments is ubiquitous. As explained below, goethite contribution is divided to action as a photo-excited semiconductor with the cells, or a heterogeneous photo-catalyst.

Goethite, in absence of $H_2O_2$ has demonstrated semiconductor properties, toward bacterial inactivation (band gap: 2.1 eV). Even more, photo-activity has also been reported [55]. Hence, $HO^\bullet$ radicals can be formed only by presence of light, and the particles that could adsorb onto the yeast surface due to negative charging [56,57] may contribute to surface holes and aid in inactivation. Furthermore, apart from the oxidative damage from the holes, the iron oxides can lead to damage on the cell surface through another semiconductor action mode. The goethite particles bound in the surface of the yeast cell are illuminated and electron excitation is following. Oxygen plays the role of electron acceptor, leading to superoxide radicals ($O_2^{\bullet-}$) and subsequent reaction with water locally produces hydroxyl radicals [18]. In our experiments, a stronger electron acceptor ($H_2O_2$) is present and the heterogeneous (Fenton with Fe-oxide as iron source) action mode is more likely to affect the inactivation process. Nevertheless, we cannot neglect the possibility of semiconductor pathways' contribution to cell damage.

In presence of $H_2O_2$, the following action modes are more prominent. Firstly, radicals' production is expected, through the excitation of electrons on the surface of the oxide, and transformation of $H_2O_2$ through the following reaction:

$$H_2O_2 + e^- \rightarrow HO^- + HO^\bullet \quad (4)$$

The other pathway includes a heterogeneous photo-Fenton mechanism for hydroxyl radical production, where $H_2O_2$ is responsible for initiating a series of reactions, leading firstly to $HO_2^\bullet$ when in contact with $Fe^{3+}$ from iron oxides' surface, reducing it to $Fe^{2+}$. $Fe^{2+}$ participates in the Fenton reaction and a cycle is initiated, described by the following reactions [18] (>Fe corresponds to the iron in the surface of the goethite particle).

$$> Fe^{3+} - OH + H_2O_2 \rightarrow > Fe^{2+} + HO_2^\bullet + H_2O \quad (5)$$

$$> Fe^{2+} + H_2O_2 \rightarrow > Fe^{3+} + HO^\bullet + OH^- \quad (6)$$

$$HO_2^\bullet \leftrightarrows H^+ + O_2^{\bullet-} \quad (7)$$

$$> Fe^{3+} - OH + HO_2^\bullet \rightarrow > Fe^{2+} + H_2O + O_2 \quad (8)$$

Finally, $Fe^{3+}$ could form exciplexes with organic compounds in the cell wall [16,58,59]. Through ligand-to-metal charge (LMCT) transfer, $Fe^{3+}$ is reduced, leading to $Fe^{2+}$ and initiating the Fenton reaction anew, in presence of light.

$$> Fe^{3+} - OH + hv \rightarrow > Fe^{2+} + HO^\bullet \quad (9)$$

### 3.1.2. Iron sulfate

$FeSO_4$ was used as a starting source of iron, where $Fe^{2+}$ is available to react with $H_2O_2$, according to the following reactions (Eqs. (10)–(13)):

$$Fe^{2+} + H_2O_2 \rightarrow Fe^{3+} + HO^\bullet + HO^- \quad (10)$$

$$Fe^{3+} + H_2O_2 \rightarrow Fe^{2+} + HO_2^\bullet + H^+ \quad (11)$$

$$Fe(OH)^{2+} + hv \rightarrow Fe^{2+} + HO^\bullet \quad (12)$$

$$Fe(COO-R)^{2+} + hv \rightarrow Fe^{2+} + CO_2 + R^\bullet \quad (13)$$

The treatment here takes place under (simulated) solar light. Hence, regeneration of the iron catalyst is taking place according to the last two equations (Eqs. (12)–(13)). Eq. (13) takes into account the possible complexes with organic by-products ($R$) deriving from the initial yeast cell wall attack, which can maintain the iron available in solution for the reaction, as follows:

$Fe^{2+}$ feeds the photo-Fenton cycle outside the cell, damaging the external membranes by the ROS produced, in the same way the HO radicals do due to heterogeneous photocatalysis with iron oxides. However, after addition of $FeSO_4$ at neutral pH, $Fe^{2+}$ has a half-life of minutes before its oxidation in $Fe^{3+}$, and the subsequent precipitation as iron oxide [60]. It also has been reported to diffuse through cell walls [16,59], increasing the inactivation efficiency through radicals' production. Contrary to bacteria, *S. cerevisiae* do not produce any siderophores to facilitate this transport, but there are (i) surface binding mechanisms, (ii) opportunistic use of siderophores from other microorganisms (in real water samples) as well as reductive and non-reductive iron transport mechanisms reported in literature [61–64].

After diffusion, although iron does not affect the carrier proteins per se, it blocks their synthesis and the transport energy resources [65]; as a result, halving of the ATPase was observed. $Fe^{2+}$ is also proposed to bind to internal membranes to participate in the internal (photo-Fenton) process and further promotes the superoxide radical production, ultimately increasing $HO^\bullet$ radical production [66]. The free iron inside saccharomyces is in $Fe^{3+}$ form [67], so reduction to $Fe^{2+}$ (and further $HO^\bullet$ production) by LMCT or by the superoxide radical is also expected [24].

Finally, since the iron is not likely to remain in solution for long [60], the heterogeneous action mode due to the formation of iron oxides is highly likely to be the driving force, after a certain point. For simplicity reasons, we do not repeat here the heterogeneous and the semiconductor action of the iron oxides as explained before; nevertheless their participation cannot be neglected.

### 3.1.3. Iron citrate

The experiments with complexed iron (by citrate ligand) simulate the mild chelating properties of naturally available iron in natural conditions. These tests presented the fastest inactivation rates for the operated pH region (pH 6.0). In principal, the optimal efficiency for the photo-Fenton reaction is found at pH 2.8. If the experiments with $FeSO_4$ were performed at that pH the efficiency would have significantly improved. However, the acidification costs for treatment and the subsequent neutralization necessary for use of the water after treatment demands viable solutions at the neutral pH. Iron citrate has been successfully used in high pH (up to 8) for pollutants' degradation [68,69] and bacterial inactivation [70], therefore its success is promising also for drinking water disinfection, since its related toxicity is very low [71]. Here, the citrate complexes lead to higher solubility and stabilization of iron cations in the solution.

In general, the action mode of citrate can be categorized as a homogeneous Fenton promoter. The generation of HO radicals is induced by photoactive $[FeOH\text{-}cit]^-$ complex, which is the main species formed at neutral pH [72]; first a LMCT transition and then a

Fenton reaction take place. The (photoactive) [FeOH-cit]$^-$ complex will generate a ligand radical (HGA2$^{\bullet -}$) and $Fe^{2+}$, which will in turn result to superoxide radical anion and HO$^\bullet$ production, respectively. This $Fe^{2+}$ can also participate in the photo-Fenton cycle mentioned before for $Fe^{2+}$ from $FeSO_4$.

#### 3.1.4. pH dependence

In order to test the efficiency of the two processes initiated by $FeSO_4$ and Fe-cit and verify the extent of homogeneous, heterogeneous action mode and side-effects of iron addition, assays in higher pH (7.5) were initiated. In Fig. 1b and c, the results for $FeSO_4$ and Fe-cit are summarized. As a rule of thumb, increase of the pH leads to faster precipitation of $Fe^{3+}$, and lower inactivation rates are expected. Nevertheless, for $FeSO_4$ the reaction duration was not affected and 45 min were necessary to completely inactivate the Saccharomyces. In pH 7.5, the oxide forms of iron are favored, and since the overall inactivation rate was not affected, it indicates the significance of the heterogeneous process in yeast inactivation.

The iron citrate inactivation was more affected by the pH increase. Since the iron and the citrate complex were synthesized by a 1:1 ratio, after the ligand to metal charge transfer and citrate's sacrifice, iron is more likely to precipitate at neutral pH, rather than re-complexing with another citrate ligand. Therefore, the homogeneous action is not affected. The difference in the inactivation rates could also probably a consequence of the side-reactions influenced by the citrate ligand, which acts as an extra target for the non-selective oxidative species generated. Our overall suggestion is that the reactions initiated by extra iron intake are limited by the pH increase, and the subsequent oxide formation.

### 3.2. Flow cytometry results—localization of damage

Very often, the viability assay through cultivation, works on the assumption that viable cells are the one able to reproduce. Hence, cultivability is the required measurement. However, Davey in her recent review emphasizes on the problematic dependence on these measurements, since microbial cells are not classified only as "live/dead", but cryptobiotic, dormant, moribund and latent states have been suggested throughout the years [73]. Therefore, flow cytometry combined with CFDA/Propidium Iodide staining has also been used in this study, for an assessment of the type and the extent of damage at yeast cells. Indicative results of one process, are presented in Fig. 2.

The staining protocol used allows the identification of living cells (appearing green in P2 quadrant) dead cells (red in P4 quadrant), as well as the unlabeled and intermediate states in quadrants P1 and P5 respectively (Fig. 2i). The green staining is an indirect indication of a living cell, since an acetoxymethyl ester of the 5-carboxyfluorescein diacetate (CFDA) added is entering the cell through the membrane, and once inside, gets hydrolyzed into acid and alcohol by non-specific enzymes (esterases) resulting in a fluorescent green stain. On the contrary, the Propidium Iodide (PI) test indicates the non-viable cells. The propidium ion is excluded from permeating the membrane and the loss of this ability suggests a loss of viability. Even so, literature suggests cases that this is not definitive [74] and live cells can get the red staining while maintaining their viability; up to 7% of these cells can still perform repair.

Fig. 2ii demonstrates the evolution of cell state in 30 min of exposure to light and the addition of the photo-Fenton reagents, at pH 5.5. This case is presented as an indicative test, and the results of the other tests will be summarized instead (Fig. 3). At time 0, 99% of the cells fall within the live state, and 1% to the other states; we remind that 30 min have preceded all experiments before illumination, to allow die-off of the most sensitive cells and acclimatization time for the rest of the cells. The intermediate cell state appearing in quadrant P5 in Fig. 2ii b and c, indicate vital cells but with compromised membrane. As the exposure time passed and cells were subjected to the actions induced by the photo-Fenton reaction, viability, as it is defined in this test, diminished within 30 min. For the rest of the tests, the conventional graphs will be presented instead. By processing the data (number of cells) on CFDA and PI staining for the first 30 or 45 min of the treatment, a correlation was found among the classic cultivability assay and the flow cytometry results (more information can be found in the Supplementary material, Fig. S2 and Table S1).

In our work, for each different test (hv, hv/$H_2O_2$, photo-Fenton with $FeSO_4$ and Fe-cit as iron sources), flow cytometry has been performed and the results were always juxtaposed with the cultivability assays presented before, for comparison. An overview of the CFDA decrease and the PI increase during the various experiments: hv, hv/$H_2O_2$, photo-Fenton ($FeSO_4$—pH 5.5 & 7.5, Fe-cit—pH 6.0 & 7.5) can be found in the Supplementary material Fig. S3, while the analytical data will be presented in Fig. 3. Following, an analytical explanation of the results of CFDA, PI and the intermediate cell state is presented, with suggestions on the inactivation mechanisms for each case. As this process is constructed in a stepwise manner, the explanations and the mechanisms suggested in the first steps (solar degradation and $H_2O_2$ oxidation), will not be repeated in the more complex systems.

#### 3.2.1. Simulated solar light

During exposure of *S. cerevisiae* to simulated solar light, the changes in esterase activity and membrane permeability were recorded and summarized in Fig. 3a. Firstly, we compared the time necessary for 50% and 90% reduction of the initial microbial load. As it appears, the cultivability assays indicate a required time somewhat higher than 30 min. However, CFDA and the PI-stained cells are almost in agreement (6% intermediate state cells) at 50 min. For 1-log reduction there is a small convergence between the two methods, with 10 min difference instead. Nevertheless, the remaining population is consistently underestimated by the cultivability assays, and viable cells that are not able to form colonies are left out of the estimation.

A critical point in this study is the timeframe of 45 min (Fig. 3a), where the number of viable cells, but with compromised membranes is the highest (11.5%). Therefore, the principal mechanism of light-induced inactivation is an internal process. More specifically, the proposed mechanism is as follows:

1) If we consider either CFDA or PI staining as the accurate viability assay, and not cultivability, the inactivation presents a shoulder, a latency (in linear scale). Therefore, there should be either an accumulation of damage before inactivation or the specific type of damage can be repaired.
2) The low accumulation of purple stains during flow cytometry (11.5% vs 26% PI-stained or generally 37.5% esterase inactive), suggests that lipid peroxidation is limited, and external proteins are rather intact. Also, it could signify that the cells are inactivated through a failure in their internal functions.
3) The above indicate that this result is probably, the effect of the actions of UVB and UVA light on nucleic/mitochondrial DNA and internal enzymes, respectively.

#### 3.2.2. hv/$H_2O_2$

The flow cytometry results for the hv/$H_2O_2$ treatment of *S. cerevisiae* are summarized in Fig. 3b. In principal, the shapes of the curves are very similar to the ones already shown during the solar-only exposure. The cultivability decreases rapidly in time, and the 4-log reduction time dropped to 30 min (instead of 60). However, the CFDA/PI staining levels presented the same lag in the beginning, with different time to reach >99.5% (30 instead of 45 min). Also, the intermediate cells were at the same percentage with the solar-

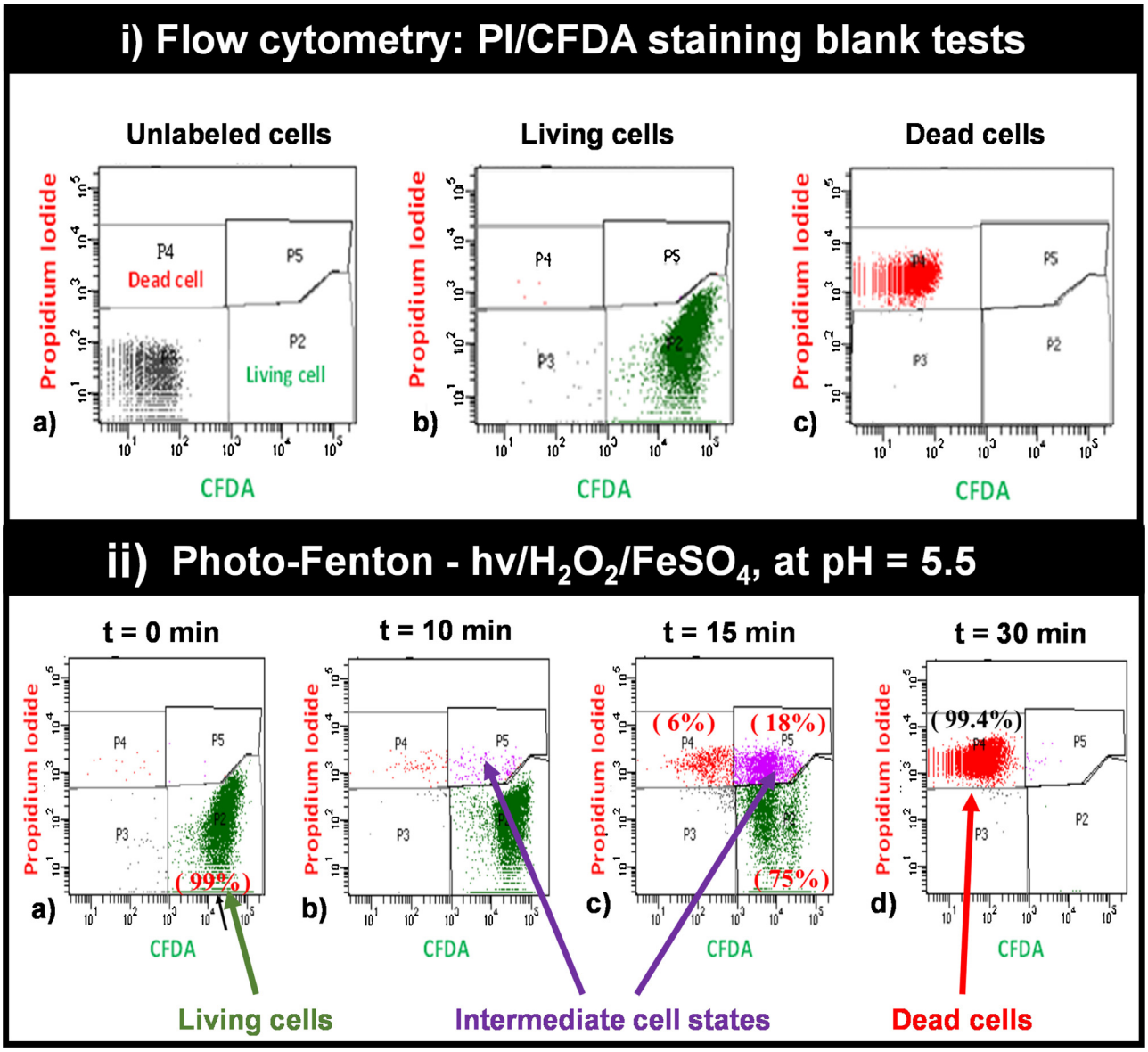


**Fig. 2.** Control tests and an indicative presentation of the flow cytometry results evolution, during photo-Fenton reaction, at pH 5.5.

only process. The main difference that modifies the inactivation mechanism lies in the higher levels of non-viable cells:

1) The latent character of inactivation indicates the necessity to accumulate damage prior to inactivate the cells. The shoulder length is again around 30 min, indicating similar accumulation of photo-induced damage.
2) The low number of intermediates could mean a low peroxidation-related killed cells. Hence, there are not many vital cells with compromised membrane.
3) In 45 min, there were significantly more inactivated cells compared with the solar-only process, with the same number of intermediate cell-states. Therefore, there is a synergy in the action of light and $H_2O_2$.
4) Since the suggested mechanism is the CPD-formation in DNA and enzymatic failure (CAT, SOD), the mutations and enzymatic activity loss could increase the permeability of the membrane, thus enhancing the $H_2O_2$ diffusion into the cell.
5) The entry of $H_2O_2$ in the cell enhances the oxidative damage, now unable to be controlled by SOD, or even more, enhancement of the internal Fenton process taking place into the cell.

*3.2.3. Photo-Fenton with $FeSO_4$, at pH 5.5 and 7.5*

Fig. 3c and d summarizes the evolution of cultivability, plus CFDA and PI staining through time. The photo-catalytic process is profoundly more efficient than solar, or hv/$H_2O_2$. The time mark of 15 min offer a solid ground for comparisons. At pH 5.5, the level of viable cells is 86%, compared with the 94% of the higher pH. Also, 4-log of cultivability loss occurs at 20 min (here recorded at 30 min for pH 7.5 due to sampling interval settings) and total inactivation takes place at 30 min.

For the samples treated at pH 5.5, there is a latent period marked with CFDA staining but probably the levels of viability are similar (Fig. 3c); the cultivability is almost equal but the marked difference is at the intermediate cells, were 5% and 40% yeasts with compromised membranes appear, for pH 5.5 and 7.5, respectively. At 20 min, the peak of intermediate cells appear for pH

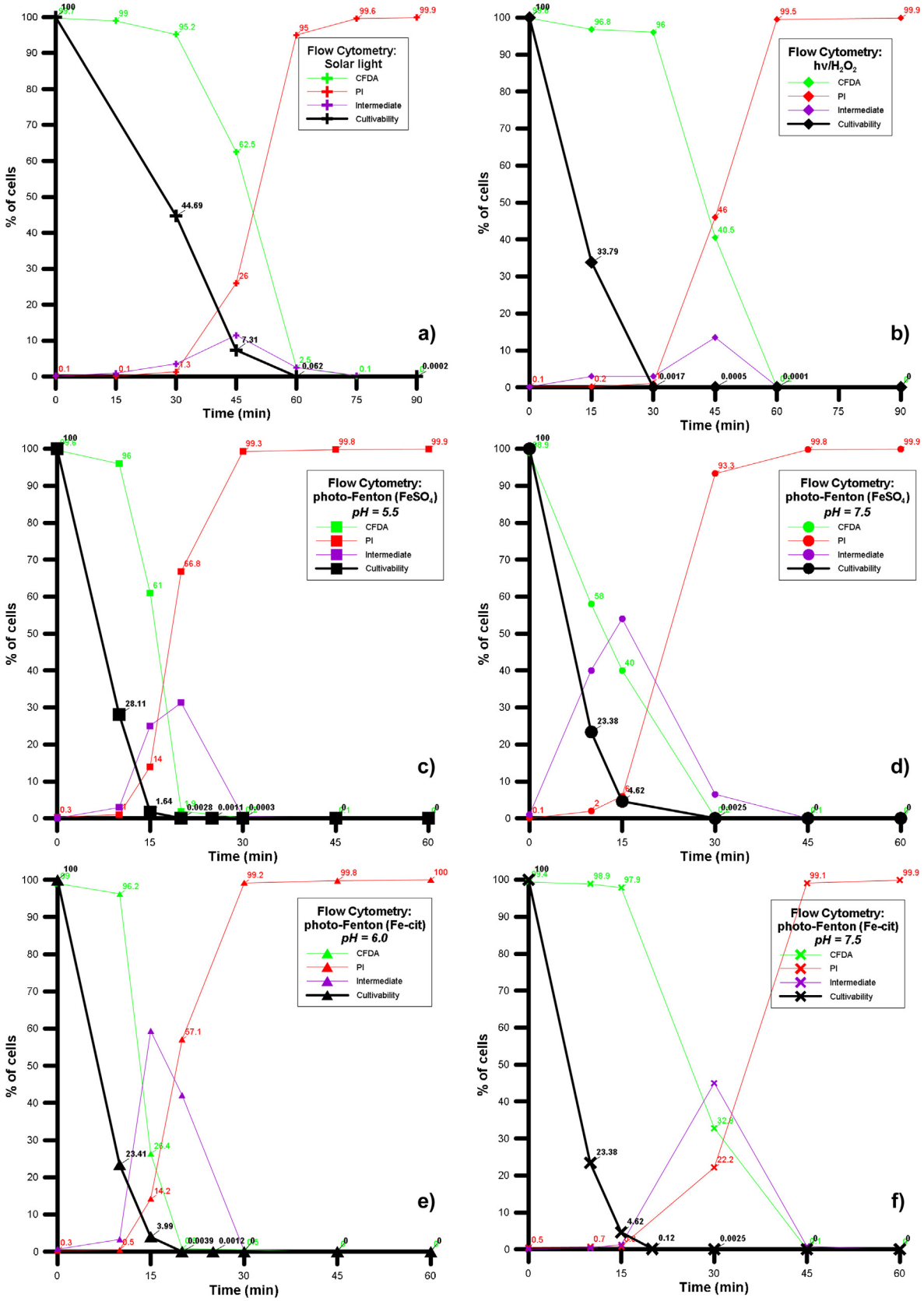


**Fig. 3.** Flow cytometry results. Control tests: (a) simulated solar light only. (b) hv/$H_2O_2$ system. $FeSO_4$-assisted photo-Fenton processes: (c) pH 5.5. (d) pH 7.5. Fe-cit-assisted photo-Fenton processes: (e) pH 6.0. f) pH 7.5. Standard deviation: <5%.

5.5, reaching 30%, and 67% dead cells (PI stain) but the striking difference at pH 7.5 is that even 5 min earlier, the peak of intermediate cells is reached, almost double in quantity (55%) and only 6% dead cells (Fig. 3d). Also at 30% where the inactivation is almost complete, the number of vital but membrane-compromised cells is higher. Hence, the proposed inactivation mechanism is as follows:

1) Although a shoulder appears in the beginning, and a build-up in damage is required, the PI stain indicates similar death rates. Therefore, at the early stage the inactivation is similar, and probably attributed to the same mechanism, of the homogeneous photo-Fenton action mode.
2) The markedly high difference after 15 min of treatment (40–50% live intact cells) but the notable difference of compromised membranes shows that the action mode is probably the external photo-Fenton, and the production of reactive oxygen species is responsible for membrane peroxidation.
3) At pH 5.5, total inactivation is achieved faster than at pH 7.5 (>99% of PI stained cells). This result is logical if the main mechanism is the external photo-Fenton, which is more profound at lower pH due to favorable form of iron and higher dissolution levels. However, the maintenance of iron as $Fe^{2+}$ and its soluble form explain the difference in intermediate cells. The diffusion of iron in the cell is higher, and the internal photo-Fenton process is enhanced. For this reason, inactivation is not heavily dependent on the external ROS action, marked by the higher red staining levels and lower membrane-compromised, compared to the process at pH 7.5.
4) At pH 7.5, iron is either participating in heterogeneous photo-Fenton reaction in form of oxides, whose efficacy is lower, or by attachment to the cell surface. The notable difference in cell integrity, due to the inflicted damage can be explained by reactions taking place at the cell surface, such as LMCT between iron forms and yeast cell wall, due to local contact-related promotion of photo-Fenton and subsequent damage at the proximity of a surface.

#### 3.2.4. Iron citrate-driven photo-Fenton reaction at pH 6.0 and 7.5

Fig. 3e and f summarize the results of the iron-citrate assisted photo-Fenton processes. As seen also in the previous section, the inactivation measured by cultivability, among the Fe-citrate-fueled experiments did not differ significantly. In Fig. 3e, at around 20–25 min of treatment, up to 4-log reduction has been achieved and at 30 min, almost complete loss of cultivability. The viability assay differs significantly from the cultivability once more. Initially, there is a lag period, 15 and 30 min for the experiments at pH 6.0 and 7.5 respectively, as measured by the loss of esterase activity, due to the similarities in the absorption spectrum among yeast and the citrate complex [70,75,76]. Even by monitoring the PI staining, an initial 10-min vs. 15-min period of latency was followed by rapid increase, to lead in 30 vs 45 min period for >99% viability loss. The peak of the intermediate states was noted at 15 min for pH 6.0, whereas at 30′ for the 7.5 pH experiments. Finally, there is a notable difference at these last time points, where for pH 6.0, at 15 min, the composition is 25% viable, 15% dead and 60% viable, but with compromised membranes. If this point characterizes the maximal damage point, for pH 7.5 at 30 min (Fig. 3f), the corresponding composition was 32%, 22% and 45%, respectively. This indicates that the damage made was rather internal, and less related with cell membrane lesions. However, this 15-min delay has to be taken into account in the mechanism suggestion that follows:

1) The lag is explained by the competition of yeast cells and the citrate complex, as they absorb in the same wavelengths. Hence, a delay in the ROS production is expected, and lower peroxidation of membranes.
2) At pH 6.0 (compared to 7.5), the solubility of iron ($Fe^{2+}$) is higher and therefore, a higher fraction is expected to participate at the homogeneous Fenton reaction. Consequently, higher ROS production and higher damage is recorded.
3) Also, the fast inactivation and the concomitant increase of dead and injured cells indicates a notable participation of the internal mechanisms of inactivation (through $Fe^{2+}$ penetration).
4) At pH 7.5, the delay expressed alters the proportions of the dead cells compared to the live ones; at the point where the intermediates reaches its maximum, more PI-stained cells appear. A heterogeneous action mode is probable as well.
5) Generally, there is less iron intake compared with the processes initiated by $FeSO_4$. This is probably attributed to the initial form of iron (complexed $Fe^{3+}$, compared to free $Fe^{2+}$). The importance of damage as depicted by the dead fractions and the time achieved is appearing to be more dependent on the internal, and less in the external photo-Fenton reactions.

### 3.3. Identification of targets—nuclear DNA, cell wall and cytoplasmic protein damage

In order to further shed light in the suggested mechanisms of *S. cerevisiae* inactivation, an assessment of the damage on nuclear DNA and the proteins of cell wall and cytoplasm, was performed. The analysis of DNA fragmentation was monitored by gel electrophoresis, and the results are summarized in Fig. 4, while Fig. 5a and b show the results of the cell wall and cytoplasmic protein damage, respectively. Protein damage is analyzed by SDS-PAGE and Coomasie blue staining. Simulated solar light only or combined with $H_2O_2$, and the two main photo-Fenton systems were compared.

In the case of simulated solar light, as it is clearly depicted (Fig. 4), DNA damage progresses over time, showing a dose-dependence with exposure. After 120 min of treatment, the fragmentation levels were too high (trace disappears). The change among the state at 60 and 120 min corroborates with the acute loss of viability recorded via the CFDA and PI staining. The cell wall proteins pool profile appears intact (Fig. 5a), and negligible degradation is was detected; the intermediate cell state was also very low, as measured by flow cytometry in Fig. 3a. Nevertheless, after 120 min there is a notable reduction of cytoplasmic proteins, which was not high until 60 min of exposure (Fig. 5b). Therefore, a double action is the probable pathway where (i) DNA is damaged severely, no repair/defense mechanisms are able to be deployed against the (mild) internal photo-Fenton action (whose damage becomes later significant), or (ii) concomitantly with the DNA destruction, the internal photo-Fenton action is becoming profound.

The addition of $H_2O_2$ in the system resulted in similar DNA damages (Fig. 4). The presence of intermediates cells cannot really be linked to DNA and protein damages visualized by electrophoresis. The results of the cell wall proteins' damage presents the first notable, but limited damage (Fig. 5a), which probably does not lead to loss of viability, but is presented only as 3% increase of intermediate cell states. However, the results of the cytoplasmic protein damage indicate the participation of $H_2O_2$ to the internal mechanisms, as the staining is less intense and more bands disappeared completely (Fig. 5b). Hence, the increased inactivation kinetics are a result of DNA damage, combined with limited cell wall peroxidation and increased internal photo-Fenton action, after the regulatory mechanisms fail to cope with the high accumulation of $H_2O_2$ and the rest of the ROS in the cell.

Adding iron to the system has a detrimental effect in all levels. First of all, DNA damages were extensive, with disappearing bands at 45 and 60 min, for $FeSO_4$ and Fe-cit respectively (Fig. 4). These

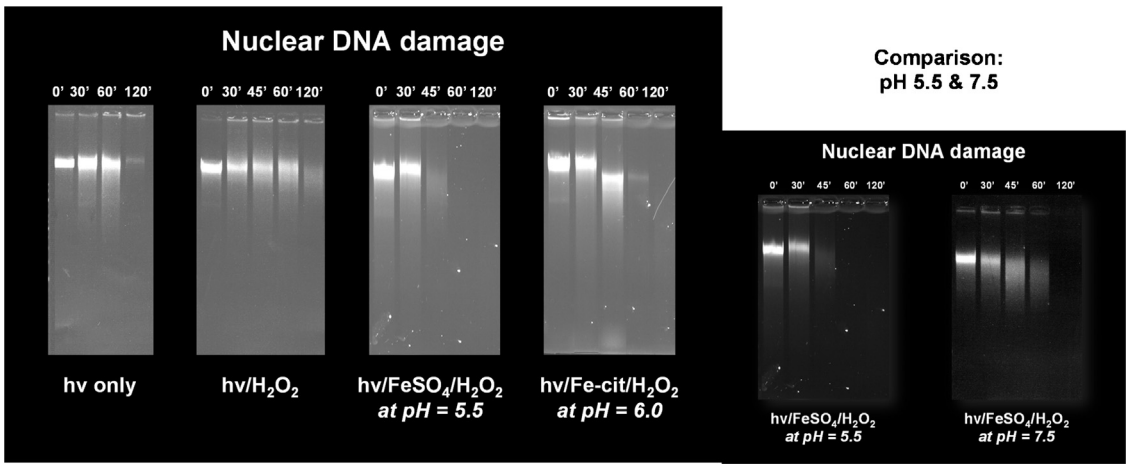


**Fig. 4.** Nuclear DNA damage in the four different systems. Comparison of the pH effect in $FeSO_4$-assisted photo-Fenton systems.

**Table 1**
Timeline of the inflicted damage in the corresponding targets of the different iron-assisted systems.

| Event | $FeSO_4$ | Fe-cit |
|---|---|---|
| Loss of cultivability | 10–20 min | 15–20–min |
| Loss of viability (by CFDA or PI) | 10–30 min | 10–30 min |
| DNA damage | 30–45 min | 45–60 min |
| Cytoplasmic proteins damage | 30–45 min | 45–60 min |
| Cell wall proteins damage | 60–120 min | 60–120 min |

time frames are significantly lower than the ones recorded for the solar and hv/$H_2O_2$ systems. Probably there is an increased loss of membrane integrity (as seen in Fig. 3c–f) and oxidative damage inside the yeast cell. As it appears on the damage of the cell wall proteins, even at time 0 the staining has a different, lighter pattern, compared with the previously presented systems. This disappearing pattern is deteriorating slowly (until 60 min) and accelerates afterwards (Fig. 5a). However, since the cytoplasmic proteins are actively getting degraded after 60 min for $FeSO_4$ and Fe-cit, the strong dependence on the internal contribution is verified (Fig. 5b).

Cultivability is lost even before the damage (at any level) is highly accumulated. Furthermore, flow cytometry suggested that the loss of viability was accelerated after 15–20 min for the iron assisted systems (Fig. 3c–f), but the protein damage is highly notable after 30 min. For the iron-supported systems, the order of events in the form of a suggested timeline can be found in Table 1. The loss of cultivability is related with the first and direct oxidative stress conditions that the cell is faced with. The simultaneous damage of DNA and cytoplasmic proteins, verify our initial hypothesis that the driving force in *S. cerevisiae* inactivation is the internal photo-Fenton process. For the two iron salts, the difference in the appearance of this effect is related with the ROS production in the system; $FeSO_4$ at pH 5.5 presented significantly higher activity. Then, as these electrophoresis processes are quantitative, the cell wall proteins appear as the last to degrade because they comprise a very big part of the total mass of the cell. This is also explained by the fact that in all figures depicting the protein damage, the bigger ones (highest kDa values) are targeted first. Finally, in order to notice oxidative damage inside the cell, only a small part of the membrane must be breached, enabling the introduction of iron into the cell (extra amount added to the diffusing one). The fact that the flow cytometry data indicate more than 50% viable but compromised membrane-cells, is the signature of the breach and the subsequent internal action.

At a higher pH for the $FeSO_4$ system, where solid Fe-oxides (goethite) is present, weaker, less active systems are involved. The DNA damages were delayed, compared to the corresponding system at 5.5 pH. However, a possible contribution of the iron oxides is noted, when the internal and external protein damage is compared. When the pH of the solution promoted the oxide formation, increased cell wall degradation was observed. Accordingly, lower internal protein damage has been recorded. The combination of these two events indicate a contribution of the iron oxides at the degradation of the cell membrane, either by promotion of local oxidative species at the surface of the (attached to the cell) iron oxide, by the oxide itself acting as a semiconductor and causing local damage to the structure, or by heterogeneous photo-catalysis in presence of $H_2O_2$.

### 3.4. Holistic proposal for the inactivation mechanism of *S. cerevisiae*

Having analyzed the cultivability and flow cytometry results, as well as the DNA and protein damages, together with an extensive literature review, a mechanism proposed for the inactivation of *S. cerevisiae* is given in Fig. 6. The four sub-figures represent distinct actions, as before: (a) simulated solar light alone (here, direct action), (b) hv/$H_2O_2$ (+indirect light actions, important at this stage), (c) $FeSO_4$-assisted (including oxides) and (d) Fe-cit-assisted photo-Fenton systems. Once again, the step-wise construction of the complex photo-Fenton mechanism is not repeated; the actions of the solar-only system and the hv/$H_2O_2$ are present in the photo-Fenton actions, but not presented again, for simplicity. Also, the references that support our observations and the subsequent suggestions are not repeated again in this section, as they were discussed before. A brief explanation on the different actions per sub-figure follows:

a) (Direct) Solar light: (1) Simulated solar light induces mutations at DNA level (e.g. CPDs, (6-4) photo-products, guanine to cytosine transversions) at both nucleic and mitochondrial genome (2). Also, mainly UVB and in a lesser extent UVA induce damage at the external cell surface (3). The cell structures suffer damage at external and internal level (4): internal groups and structural functions (enzymes, clusters, proteins etc) are physically affected by the direct illumination. Cell death can be the final outcome of the loss of viability.
b) (Indirect) hv/$H_2O_2$: Light affects internal enzymes, such as superoxide dismutase (SOD) and peroxidases, such as catalase, oxidase etc. (1) and (2). As a result, the internal respiratory chain is affected, with subsequent $H_2O_2$ and $O_2^{\bullet -}$ accumulation. Since Fe/S clusters are affected, release of iron is expected, and an

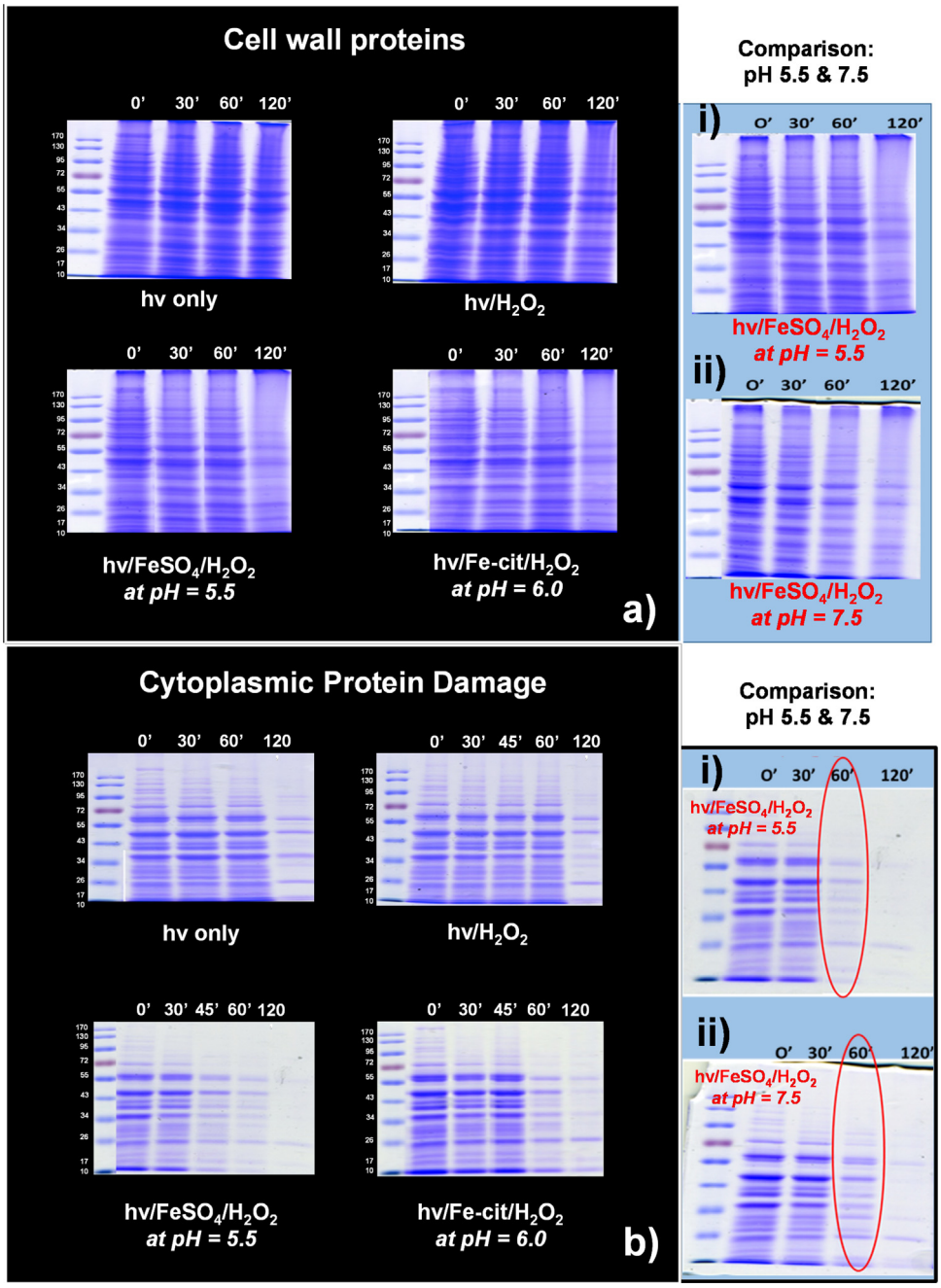


**Fig. 5.** Cell wall (a) and cytoplasmic proteins damage (b) in the four different systems. (i and ii): comparison of the pH effect in $FeSO_4$-assisted photo-Fenton systems.

internal Fenton mechanism is initiated with the hydroxyl radicals damaging internally the cell. $H_2O_2$ plays both the role of oxidant for $Fe^{2+}$ and the reductive for $Fe^{3+}$, and since light is present, internal photo-Fenton is taking place. The superoxide radical also participates in iron reduction and the internal oxidation actions. As far as the external actions are concerned, mild peroxidation of the external cell wall proteins at small extent is expected (3) and possible penetration of $H_2O_2$ into the cell (4). These actions further enhance the internal photo-Fenton actions.

c) $FeSO_4$-assisted photo-Fenton: The addition of $FeSO_4$ in the solution provides (for a limited period of time) $Fe^{2+}$, which produces radicals externally (1). $Fe^{3+}$ complexes are reduced by light, further producing hydroxyl radicals and $Fe^{2+}$. The rupture of the cell wall can allow the penetration of $Fe^{2+}$ and $Fe^{3+}$ into the cell, enhancing the Fenton reactions taking place inside the cell (2). Also, the iron transport mechanisms carry $Fe^{2+}$ and $Fe^{3+}$ into the cell, to maintain homeostasis, with the same effect as before (3). However, the presence of dissolved oxygen in the sample and the near-neutral pH cause the oxidation of iron to goethite and lepidocrocite; the heterogeneous Fenton action is initiated (4). The attachment of the (positively charged) iron to the (negatively charged) cell wall induces local damage to the cell through either (5) a photo-assisted reduction of $Fe^{3+}$ (LMCT) on cell wall and the initiation of a photo-Fenton action (since $H_2O_2$ and light are present and $Fe^{2+}$ is produced) or (6) semiconductor action mode by the iron oxide, which includes oxidative damage from the hole ($h^+$) and the excitation of electrons ($e^-$). These electrons, in presence of oxygen or $H_2O_2$, acting as electron acceptors, gen-

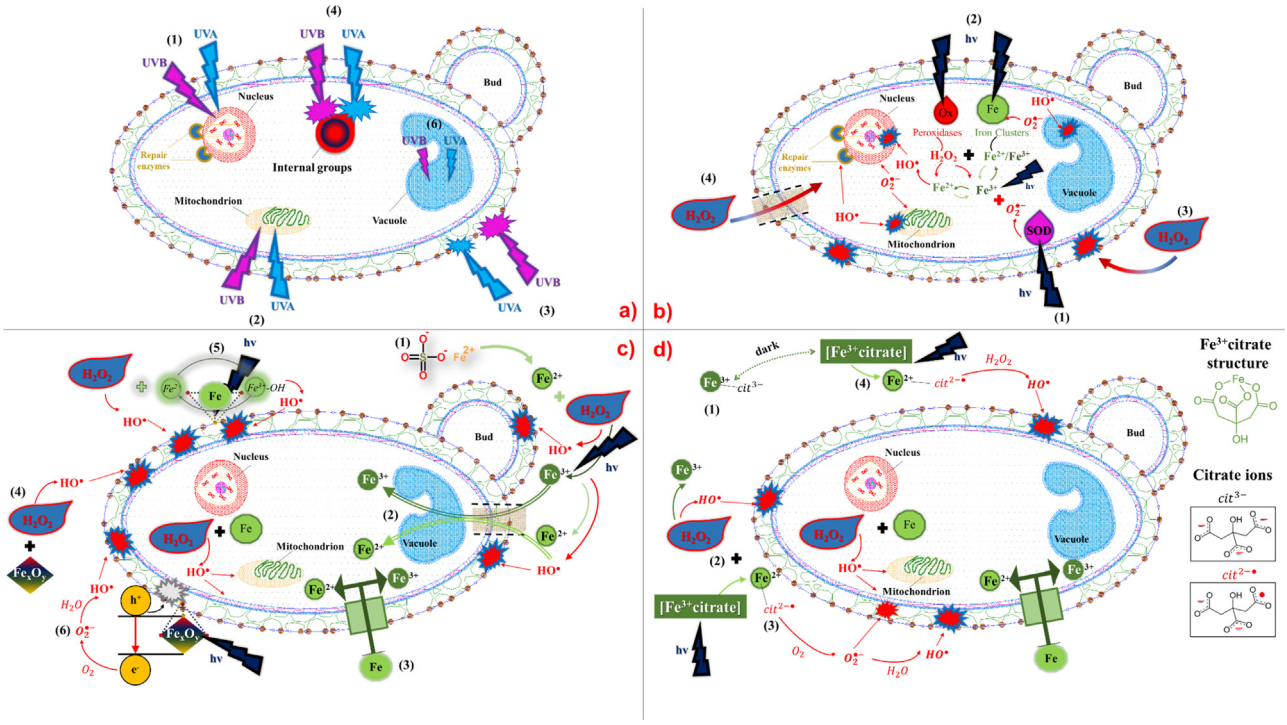


**Fig. 6.** Mechanistic proposition of the pathways toward yeast cell inactivation. (a) (direct) simulated solar light. (b) (Indirect) hv/$H_2O_2$. (c) $FeSO_4$-assisted photo-Fenton process. (d) Fe-cit-assisted photo-Fenton process.

erate ROS that cause extra oxidative damage in the exterior of the cell.

d) Fe-cit-assisted photo-Fenton: Iron citrate is stable in water, in absence of light (equilibrium 1). Light on the Fe-citrate, on the other hand, induces another pathway, involving LMCT and a [$Fe^{2+}$—9472;$cit^{2-}$] product. Its dissociation gives $Fe^{2+}$ and $cit^{2-\bullet}$, which can participate in the Fenton reaction (2) and formation of superoxide radical anions (3), respectively. Alternatively, the $cit^{2-\bullet}$ can react with $H_2O_2$ (4). The end-product is a hydroxyl radical, which inflicts external damage to the cell.

## 4. Conclusions

A eukaryotic, unicellular microorganism (*S. cerevisiae*) was subjected to a multi-level, systematic investigation on its inactivation mechanisms. The contribution of photo-Fenton and its constituents were put under study, and light was shed on the separate or synergistic pathways participating in yeast inactivation.

The cultivability results indicated the best conditions and starting iron forms, to achieve the best inactivation rates. Furthermore, flow cytometry data coupled with the electrophoresis data on DNA and protein suggested the pathways toward inactivation. A significant contribution of the internal photo-Fenton process was measured, in addition to the external oxidative stress by the ROS produced.

In principal, the action of light was monitored to affect mainly the DNA, and secondarily, the internal proteins. The sequence of events suggests a photocatalytic-like induction of damage. When $H_2O_2$ was added to the system, the non-viable cells were a result of increased internal photocatalytic reactions, when compared with bare light. The addition of iron greatly enhanced the process, reducing the inactivation time significantly. The generation of ROS inside and outside the cell reduced the viability by destroying DNA and internal proteins, and when the process was prolonged, total destruction of the cell was monitored.

According to the pH levels, iron oxides participate in heterogeneous pathways. Efficient photo-Fenton inactivation was observed at pH 7.5, and in cellular level, a mixed mode between the diffusion of iron into the cell and the damage caused from iron particles attached to the surface of the cell. Finally, iron citrate, a relatively cheap organic complex was investigated, to increase the applicability of the process. The significant inactivation measured indicates promising application potentials.

In overall, a wide view into the pathway of *S. cerevisiae* inactivation was given, helping understand the inactivation of more complex microorganisms. Nevertheless, its complexity did not offer great resistance against the photo-Fenton reaction, but can offer great insight on the function of eukaryotic cells when present in similar oxidative stresses.

## Acknowledgments

The authors wish to thank the Swiss National Science Foundation for financial support through the program “Research partnership with developing countries” (Project No. IZ70Z0_131312/1-2). Also the authors acknowledge the Swiss Agency for Development and Cooperation (SDC) and the Swiss National Foundation for the Research for Development Grant, for the funding through the project “Treatment of the hospital wastewaters in Côte d’Ivoire and in Colombia by advanced oxidation processes” (Project No. 146919).

## Appendix A. Supplementary data

Supplementary data associated with this article can be found, in the online version, at http://dx.doi.org/10.1016/j.apcatb.2015.12.016.

## References


[1] Black, C. Veatch, White's Handbook of Chlorination and Alternative Disinfectants, John Wiley & Sons, Inc., 2010, pp. 363–403.
[2] P. Verlicchi, M. Al Aukidy, A. Galletti, M. Petrovic, D. Barceló, Sci. Total Environ. 430 (2012) 109–118.
[3] T. Schwartz, W. Kohnen, B. Jansen, U. Obst, FEMS Microbiol. Ecol. 43 (2003) 325–335.
[4] C.S. Li, W.C. Chia, P.S. Chen, J. Environ. Sci. Health Part A 42 (2007) 195–203.
[5] T. Prado, D.M. Silva, W.C. Guilayn, T.L. Rose, A.M.C. Gaspar, M.P. Miagostovich, Water Res. 45 (2011) 1287–1297.
[6] E. Emmanuel, G. Keck, J.-M. Blanchard, P. Vermande, Y. Perrodin, Environ. Int. 30 (2004) 891–900.
[7] J. Lienert, M. Koller, J. Konrad, C.S. McArdell, N. Schuwirth, Environ. Sci. Technol. 45 (2011) 3848–3857.
[8] K.G. McGuigan, R.M. Conroy, H.-J. Mosler, M. du Preez, E. Ubomba-Jaswa, P. Fernandez-Ibañez, J. Hazard. Mater. 235 (2012) 29–46.
[9] K.E. Gibson, Curr. Opini. Virol. 4 (2014) 50–57.
[10] C. Ruales-Lonfat, N. Benítez, A. Sienkiewicz, C. Pulgarín, Appl. Catal. B: Environ. 160 (2014) 286–297.
[11] C. Comninellis, A. Kapalka, S. Malato, S.A. Parsons, I. Poulios, D. Mantzavinos, J. Chem. Technol. Biotechnol. 83 (2008) 769–776.
[12] J. Poyatos, M. Muñio, M. Almecija, J. Torres, E. Hontoria, F. Osorio, Water Air Soil Pollu. 205 (2010) 187–204.
[13] A.-G. Rincón, C. Pulgarin, App. Catal. B: Environ. 63 (2006) 222–231.
[14] J. Ndounla, D. Spuhler, S. Kenfack, J. Wéthé, C. Pulgarin, Appl. Catal. B: Environ. 129 (2013) 309–317.
[15] J. Ndounla, S. Kenfack, J. Wéthé, C. Pulgarin, Appl. Catal. B: Environ. 148 (2014) 144–153.
[16] D. Spuhler, J.A. Rengifo-Herrera, C. Pulgarin, Appl. Catal. B: Environ. 96 (2010) 126–141.
[17] E. Ortega-Gómez, B.E. García, M.B. Martín, P.F. Ibáñez, J.S. Pérez, Catal. Today 209 (2013) 195–200.
[18] C. Ruales-Lonfat, J. Barona, A. Sienkiewicz, M. Bensimon, J. Vélez-Colmenares, N. Benítez, C. Pulgarín, Appl. Catal. B: Environ. 166 (2015) 497–508.
[19] E. Ortega-Gómez, M.B. Martín, A. Carratalà, P.F. Ibañez, J.S. Pérez, C. Pulgarín, Appl. Catal. B: Environ. 174 (2015) 395–402.
[20] N.E. Brinkman, R.A. Haugland, L.J. Wymer, M. Byappanahalli, R.L. Whitman, S.J. Vesper, Appl. Environ. Microbiol. 69 (2003) 1775–1782.
[21] M.S. Park, J.E. Eom, J.J. Fong, Y.W. Lim, J. Microbiol. 53 (2015) 219–225.
[22] S. Pigeot-Remy, P. Real, F. Simonet, C. Hernandez, C. Vallet, J.C. Lazzaroni, S. Vacher, C. Guillard, Appl. Catal. B: Environ. 134–135 (2013) 167–173.
[23] S. Thabet, F. Simonet, M. Lemaire, C. Guillard, P. Cotton, Appl. Environ. Microbiol. 80 (2014) 7527–7535.
[24] M.D. Temple, G.G. Perrone, I.W. Dawes, Trends Cell Biol. 15 (2005) 319–326.
[25] C. Sichel, M. De Cara, J. Tello, J. Blanco, P. Fernández-Ibáñez, Appl. Catal. B: Environ. 74 (2007) 152–160.
[26] C. Sichel, P. Fernández-Ibáñez, M. De Cara, J. Tello, Water Res. 43 (2009) 1841–1850.
[27] S. Thabet, M. Weiss-Gayet, F. Dappozze, P. Cotton, C. Guillard, Appl. Catal. B: Environ. 140 (2013) 169–178.
[28] E. Antonini, H.-J. Vidic, Complejo de hierro-citrato, procedimiento para su fabricación y su aplicación farmacéutica., In: Oficina Española de Patentes y Marcas (Ed.) Spanish 1994.
[29] E.F. Sambrook, Molecular Cloning: A Laboratory Manual, 2nd ed., Cold Spring Harbor laboratory, Cold Spring Harbor, New York, 1992.
[30] U.K. Laemmli, Nature 227 (1970) 680–685.
[31] I. Oyane, T. Takeda, Y. Oda, T. Sakata, M. Furuta, K. Okitsu, Y. Maeda, R. Nishimura, Ultrason. Sonochem. 16 (2009) 532–536.
[32] C.M. Grant, K.A. Quinn, I.W. Dawes, Mol. Cell. Biol. 19 (1999) 2650–2656.
[33] E. Cabiscol, E. Piulats, P. Echave, E. Herrero, J. Ros, J. Biol. Chem. 275 (2000) 27393–27398.
[34] V.M. Costa, M.A. Amorim, A. Quintanilha, P. Moradas-Ferreira, Free Radi. Biol. Med. 33 (2002) 1507–1515.
[35] A. Sousa-Lopes, F. Antunes, L. Cyrne, H. Marinho, FEBS Lett. 578 (2004) 152–156.
[36] K. Takeshita, J. Shibato, T. Sameshima, S. Fukunaga, S. Isobe, K. Arihara, M. Itoh, Int. J. Food Microbiol. 85 (2003) 151–158.
[37] S. Giannakis, E. Darakas, A. Escalas-Cañellas, C. Pulgarin, Chem. Eng. J. 281 (2015) 588–598.
[38] S. Giannakis, E. Darakas, A. Escalas-Cañellas, C. Pulgarin, Photochem. Photobiol. Sci. (2015).
[39] C. Sichel, J. Tello, M. De Cara, P. Fernández-Ibáñez, Catal. Today 129 (2007) 152–160.
[40] S. Giannakis, E. Darakas, A. Escalas-Canellas, C. Pulgarin, J. Photochem. Photobiol. A: Chem. 280 (2014) 14–26.
[41] S. Giannakis, E. Darakas, A. Escalas-Canellas, C. Pulgarin, J. Photochem. Photobiol. A: Chem. 290 (2014) 43–53.
[42] M. Schenk, S. Raffellini, S. Guerrero, G.A. Blanco, S.M. Alzamora, LWT—Food Sci. Technol. 44 (2011) 191–198.
[43] G.P. Pfeifer, Y.-H. You, A. Besaratinia, Mutat. Res./Fundam. Mol. Mech. Mutagen. 571 (2005) 19–31.
[44] P.E. Hockberger, T.A. Skimina, V.E. Centonze, C. Lavin, S. Chu, S. Dadras, J.K. Reddy, J.G. White, Proc. Natl. Acad. Sci. U. S. A. 96 (1999) 6255–6260.
[45] C. Pourzand, R.D. Watkin, J.E. Brown, R.M. Tyrrell, Proc. Natl. Acad. Sci. U. S. A. 96 (1999) 6751–6756.
[46] J. De Freitas, H. Wintz, J.H. Kim, H. Poynton, T. Fox, C. Vulpe, Biometals 16 (2003) 185–197.
[47] C. Lindberg, G. Horneck, J. Photochem. Photobiol. B: Biol. 11 (1991) 69–80.
[48] K. Schenk-Meuser, K. Pawlowsky, J. Kiefer, J. Photochem. Photobiol. B: Biol. 14 (1992) 231–245.
[49] R. Del Carratore, C. Della Croce, M. Simili, E. Taccini, M. Scavuzzo, S. Sbrana, Mutat. Res./Genet. Toxicol. Environ. Mutagen. 513 (2002) 183–191.
[50] K. Chen, N. Liang, J. Yang, H. Zhao, UV-B irradiation regulates apoptosis in yeast, in: Proceedings of the 2012 International Conference on Applied Biotechnology (ICAB 2012), Springer, 2014, pp. 1869–1879.
[51] A. Zapata, I. Oller, L. Rizzo, S. Hilgert, M. Maldonado, J. Sánchez-Pérez, S. Malato, Appl. Catal. B: Environ. 97 (2010) 292–298.
[52] K. Keyer, A.S. Gort, J.A. Imlay, J. Bacteriol. 177 (1995) 6782–6790.
[53] J. Xu, N. Sahai, C.M. Eggleston, M.A. Schoonen, Earth Planet. Sci. Lett. 363 (2013) 156–167.
[54] J.A. Imlay, Annu. Rev. Biochem. 77 (2008) 755.
[55] J.K. Leland, A.J. Bard, J. Phys. Chem. 91 (1987) 5076–5083.
[56] C.A. Dunlap, G. Biresaw, M.A. Jackson, Colloids and Surfa. B: Biointerfaces 46 (2005) 261–266.
[57] M. Polo-López, P. Fernández-Ibáñez, I. García-Fernández, I. Salgado-Tránsito, C. Sichel, J. Chem. Technol. Biotechnol. 85 (2010) 1038–1048.
[58] M. Polo-López, I. Oller, P. Fernández-Ibáñez, Catal. Today 209 (2013) 181–187.
[59] M. Polo-López, M. Castro-Alférez, I. Oller, P. Fernández-Ibáñez, Chem. Eng. J. 257 (2014) 122–130.
[60] J.F. Barona, D.F. Morales, L.F. González-Bahamón, C. Pulgarín, L.N. Benítez, Appl. Catal. B: Environ. 165 (2015) 620–627.
[61] R. Stearman, D.S. Yuan, Y. Yamaguchi-Iwai, R.D. Klausner, A. Dancis, Science 271 (1996) 1552–1557.
[62] C.-W. Yun, T. Ferea, J. Rashford, O. Ardon, P.O. Brown, D. Botstein, J. Kaplan, C.C. Philpott, J. Biol. Chem. 275 (2000) 10709–10715.
[63] E. Lesuisse, P.-L. Blaiseau, A. Dancis, J.-M. Camadro, Microbiology 147 (2001) 289–298.
[64] F. Gaensly, G. Picheth, D. Brand, T. Bonfim, Braz. J. Microbiol. 45 (2014) 491–494.
[65] U. Khansuwan, A. Kotyk, Folia Microbiol. 45 (2000) 515–520.
[66] K. Sigler, G. Gille, V. Vacata, N. Stadler, M. Höfer, Folia Microbiol. 43 (1998) 361–367.
[67] C. Srinivasan, A. Liba, J.A. Imlay, J.S. Valentine, E.B. Gralla, J. Biol. Chem. 275 (2000) 29187–29192.
[68] H. Katsumata, S. Kaneco, T. Suzuki, K. Ohta, Y. Yobiko, J. Photochem. Photobiol. A: Chem. 180 (2006) 38–45.
[69] A.G. Trovó, R.F. Nogueira, J. Braz. Chem. Soc. 22 (2011) 1033–1039.
[70] C. Ruales-Lonfat, J.F., Barona, A., Sienkiewicz, J. Velez-Colmenares, N., Benitez, C. Pulgarin, Appl. Catal. B: Environ., (unpublished data: under review).
[71] M. Silva, A. Trovó, R. Nogueira, J. Photochem. Photobiol. A: Chem. 191 (2007) 187–192.
[72] Y. Chen, Z. Liu, Z. Wang, M. Xue, X. Zhu, T. Tao, J. Hazard. Mater. 194 (2011) 202–208.
[73] H.M. Davey, Appl. Environ. Microbiol. 77 (2011) 5571–5576.
[74] H.M. Davey, P. Hexley, Environ. Microbiol. 13 (2011) 163–171.
[75] S. Ułaszewski, T. Mamouneas, W.-K. Shen, P.J. Rosenthal, J.R. Woodward, V.P. Cirillo, L.N. Edmunds, J. Bacteriol. 138 (1979) 523–529.
[76] J.B. Robertson, C.R. Davis, C.H. Johnson, Proc. Natl. Acad. Sci. U. S. A. 110 (2013) 21130–21135.